Available online at www.sciencedirect.com
SCIENCE DIRECT®
Computers and Structures 83 (2005) 1526–1535
Computers & Structures
www.elsevier.com/locate/compstruc

A meshfree method based on the peridynamic model of solid mechanics

S.A. Silling [a,*], E. Askari [b]

[a] Department of Computational Physics, MS-0378, Sandia National Laboratories, Albuquerque, NM 87185-0378, United States
[b] Math Group, Boeing Phantom Works, P.O. Box 3707, MC 7L-25 Seattle, WA 98124-2207, United States

Accepted 28 November 2004
Available online 21 March 2005

Abstract

An alternative theory of solid mechanics, known as the peridynamic theory, formulates problems in terms of integral equations rather than partial differential equations. This theory assumes that particles in a continuum interact with each other across a finite distance, as in molecular dynamics. Damage is incorporated in the theory at the level of these two-particle interactions, so localization and fracture occur as a natural outgrowth of the equation of motion and constitutive models. A numerical method for solving dynamic problems within the peridynamic theory is described. Accuracy and numerical stability are discussed. Examples illustrate the properties of the method for modeling brittle dynamic crack growth.

1. Introduction

Numerical prediction of crack growth is a long-standing problem in computational mechanics. The difficulty inherent in this problem arises from the basic incompatibility of cracks with the partial differential equations that are used in the classical theory of solid mechanics. The spatial derivatives needed for these partial differential equations to make sense do not exist on a crack tip or surface. Therefore, any numerical method derived from these equations inherits this difficulty in modeling cracks. In spite of the progress that has been made in developing meshfree methods aimed at modeling fracture, for example [1–6], such meshfree techniques generally require some special method of evaluating the spatial derivatives on each crack surface. They also require supplemental relations that govern the initiation of cracks, as well as their growth velocity and direction. These relations must be applied along each crack tip, leading to inherent complexity of the method, particularly when multiple cracks occur and interact in three dimensions. It is also possible to construct constitutive models that lead asymptotically to localization in a continuum, for example [7], but these techniques do not entirely avoid the need for special treatment of a crack after it forms.

As an attempt at improving this situation, a theory of solid mechanics has been proposed that does not require spatial derivatives to be evaluated within a body [8–13]. This theory, known as the *peridynamic* theory, instead uses integral equations. The objective is to reformulate the basic mathematical description of solid mechanics in such a way that the identical equations hold either on or off of a discontinuity such as a crack. The present paper discusses a numerical approach to solving

* Corresponding author. Tel.: +5058443973.
E-mail address: sasilli@sandia.gov (S.A. Silling).

0045-7949/$ - see front matter © 2005 Elsevier Ltd. All rights reserved.
doi:10.1016/j.compstruc.2004.11.026

initial-value problems within this theory, with particular application to fracture and failure.

2. Peridynamic model of a continuum

The peridynamic theory may be thought of as a continuum version of molecular dynamics. The acceleration of any particle at $\mathbf{x}$ in the reference configuration at time t is found from

$$\rho\ddot{\mathbf{u}}(\mathbf{x},t) = \int_{\mathscr{H}_\mathbf{x}} \mathbf{f}(\mathbf{u}(\mathbf{x}',t) - \mathbf{u}(\mathbf{x},t), \mathbf{x}' - \mathbf{x}) \mathrm{d}V_{\mathbf{x}'} + \mathbf{b}(\mathbf{x},t), \tag{1}$$

where $\mathscr{H}_\mathbf{x}$ is a neighborhood of $\mathbf{x}$, $\mathbf{u}$ is the displacement vector field, $\mathbf{b}$ is a prescribed body force density field, ρ is mass density in the reference configuration, and $\mathbf{f}$ is a *pairwise force function* whose value is the force vector (per unit volume squared) that the particle $\mathbf{x}'$ exerts on the particle $\mathbf{x}$. In the following discussion, we denote the relative position of these two particles in the reference configuration by $\boldsymbol{\xi}$:

$$\boldsymbol{\xi} = \mathbf{x}' - \mathbf{x}, \tag{2}$$

and their relative displacement by $\boldsymbol{\eta}$

$$\boldsymbol{\eta} = \mathbf{u}(\mathbf{x}',t) - \mathbf{u}(\mathbf{x},t). \tag{3}$$

Note that $\boldsymbol{\eta} + \boldsymbol{\xi}$ represents the *current* relative position vector between the particles.

The direct physical interaction (which occurs through unspecified means) between the particles at $\mathbf{x}$ and $\mathbf{x}'$ will be called a *bond*, or, in the special case of an elastic interaction to be defined below, a *spring*. The concept of a bond that extends over a finite distance is a fundamental difference between the peridynamic theory and the classical theory, which is based on the idea of contact forces (interactions between particles that are in direct contact with each other).

It is convenient to assume that for a given material there is a positive number δ, called the *horizon*, such that

$$|\boldsymbol{\xi}| > \delta \Rightarrow \mathbf{f}(\boldsymbol{\eta},\boldsymbol{\xi}) = \mathbf{0} \quad \forall \boldsymbol{\eta}. \tag{4}$$

In other words, the particle $\mathbf{x}$ cannot "see" beyond this horizon. For the remainder of this discussion, $\mathscr{H}_\mathbf{x}$ will denote the spherical neighborhood of $\mathbf{x}$ in $\mathscr{R}$ with radius δ (Fig. 1).

The pairwise force function $\mathbf{f}$ is required to have the following properties:

$$\mathbf{f}(-\boldsymbol{\eta},-\boldsymbol{\xi}) = -\mathbf{f}(\boldsymbol{\eta},\boldsymbol{\xi}) \quad \forall \boldsymbol{\eta},\boldsymbol{\xi}, \tag{5}$$

which assures conservation of linear momentum, and

$$(\boldsymbol{\xi}+\boldsymbol{\eta}) \times \mathbf{f}(\boldsymbol{\eta},\boldsymbol{\xi}) = \mathbf{0} \quad \forall \boldsymbol{\eta},\boldsymbol{\xi}, \tag{6}$$

which assures conservation of angular momentum. The latter equation means that the force vector between these particles is parallel to their current relative position vector.

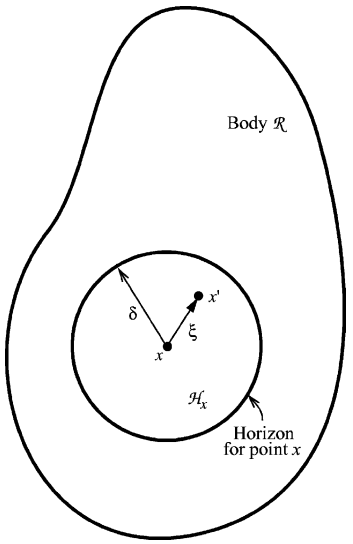

Fig. 1. Each point $\mathbf{x}$ in the body interacts directly with points in the sphere $\mathscr{H}_\mathbf{x}$ through *bonds*.

A material is said to be *microelastic* if the pairwise force function is derivable from a scalar *micropotential* w:

$$\mathbf{f}(\boldsymbol{\eta},\boldsymbol{\xi}) = \frac{\partial w}{\partial \boldsymbol{\eta}}(\boldsymbol{\eta},\boldsymbol{\xi}) \quad \forall \boldsymbol{\xi},\boldsymbol{\eta}. \tag{7}$$

The micropotential is the energy in a single bond and has dimensions of energy per unit volume squared. The energy per unit volume in the body at a given point (i.e., the local strain energy density) is therefore found from

$$W = \frac{1}{2}\int_{\mathscr{H}_\mathbf{x}} w(\boldsymbol{\eta},\boldsymbol{\xi}) \mathrm{d}V_{\xi}. \tag{8}$$

The factor of 1/2 appears because each endpoint of a bond "owns" only half the energy in the bond.

If a body is composed of a microelastic material, work done on it by external forces is stored in recoverable form in much the same way as in the classical theory of elasticity. Furthermore, it can be shown that the micropotential depends on the relative displacement vector $\boldsymbol{\eta}$ only through the *scalar* distance between the deformed points. Thus, there is a scalar-valued function $\hat{w}$ such that

$$\hat{w}(y,\boldsymbol{\xi}) = w(\boldsymbol{\eta},\boldsymbol{\xi}) \quad \forall \boldsymbol{\xi},\boldsymbol{\eta} \quad y = |\boldsymbol{\eta}+\boldsymbol{\xi}|. \tag{9}$$

Therefore, the interaction between any two points in a microelastic material may be thought of as an elastic (and possibly nonlinear) spring. The spring properties may depend on the separation vector $\boldsymbol{\xi}$ in the reference configuration.

Anisotropy may be included in the microelastic response through this dependence on the direction of $\boldsymbol{\xi}$.

For example, in a model of a unidirectional fiber-reinforced composite material in which the fibers are parallel to a given unit vector $\mathbf{g}$, one might take

$$\hat{w}(y,\boldsymbol{\xi}) = \beta^2 \hat{w}_{\text{fiber}}(y, |\boldsymbol{\xi}|) + (1-\beta^2)\hat{w}_{\text{matrix}}(y, |\boldsymbol{\xi}|), \quad \beta = \mathbf{g}\cdot\boldsymbol{\xi}/|\boldsymbol{\xi}|, \tag{10}$$

which explicitly supplies the dependence of bond energy on the bond direction.

Combining (7) and (9) and differentiating the latter with respect to the components of $\boldsymbol{\eta}$ leads to

$$\mathbf{f}(\boldsymbol{\eta},\boldsymbol{\xi}) = \frac{\boldsymbol{\xi}+\boldsymbol{\eta}}{|\boldsymbol{\xi}+\boldsymbol{\eta}|} f(|\boldsymbol{\xi}+\boldsymbol{\eta}|,\boldsymbol{\xi}) \quad \forall \boldsymbol{\xi},\boldsymbol{\eta}, \tag{11}$$

where f is the scalar-valued function defined by

$$f(y,\boldsymbol{\xi}) = \frac{\partial \hat{w}}{\partial y}(y,\boldsymbol{\xi}) \quad \forall y,\boldsymbol{\eta}. \tag{12}$$

This satisfies the requirements (5) and (6) provided

$$\hat{w}(y,-\boldsymbol{\xi}) = \hat{w}(y,\boldsymbol{\xi}) \quad \forall y,\boldsymbol{\xi}, \tag{13}$$

which will henceforth be assumed.

The relation (11), together with the equation of motion (1), essentially contain the totality of the peridynamic model for a nonlinear microelastic material. In particular, note that the issue of how to treat rigid rotation does not arise in this formulation because y is invariant under rotation of the body. Similarly, objectivity of a constitutive model is not an issue in this approach.

A linearized version of the theory for a microelastic material takes the form

$$\mathbf{f}(\boldsymbol{\eta},\boldsymbol{\xi}) = \mathbf{C}(\boldsymbol{\xi})\boldsymbol{\eta} \quad \forall \boldsymbol{\xi},\boldsymbol{\eta} \tag{14}$$

where $\mathbf{C}$ is the material's *micromodulus* function, whose value is a second-order tensor given by

$$\mathbf{C}(\boldsymbol{\xi}) = \frac{\partial \mathbf{f}}{\partial \boldsymbol{\eta}}(\mathbf{0},\boldsymbol{\xi}) \quad \forall \boldsymbol{\xi}. \tag{15}$$

This function inherits the following requirement from (5):

$$\mathbf{C}(-\boldsymbol{\xi}) = \mathbf{C}(\boldsymbol{\xi}) \quad \forall \boldsymbol{\xi}. \tag{16}$$

The properties of $\mathbf{C}$ are discussed in detail in [8].

Weckner [13] observed that certain elements of the linear peridynamic theory just described, particularly in one dimension, have been reported in earlier investigations by Kunin [14] and by Rogula [15]. These methods apparently were proposed as a method for the study of the properties of linear elastic materials with microstructure rather than as a more general technique for modeling deformation and failure of engineering structures. It should also be noted that the peridynamic model is a type of nonlocal theory, in the sense that particles separated by a finite distance can interact directly. To draw a distinction between this and other nonlocal theories, note that most nonlocal theories involve a requirement for averaging some measure of strain within some neighborhood of a material particle. The present method differs from such nonlocal theories in that it does not use strain, which by definition involves partial derivatives of displacement. A nonlocal theory that has been successfully applied to crack tip problems was proposed by Eringen [16]. Another nonlocal approach that has been developed for materials like concrete is described by Ozbolt and Bazant [17].

3. Constitutive modeling

With a view toward modeling spontaneous fracture in a deforming body, a notion of failure will be included in the nonlinear microelastic material model previously described. It will be assumed for simplicity that the scalar bond force f depends only on the *bond stretch*, defined by

$$s = \frac{|\boldsymbol{\xi}+\boldsymbol{\eta}| - |\boldsymbol{\xi}|}{|\boldsymbol{\xi}|} = \frac{y - |\boldsymbol{\xi}|}{|\boldsymbol{\xi}|}. \tag{17}$$

Thus s is positive when the bond is in tension. Note that such a material is isotropic, since there is no dependence of f on the direction of $\boldsymbol{\xi}$.

The simplest way to introduce failure into a constitutive model is by allowing bonds (springs) to break when they are stretched beyond a predefined limit. After bond failure, there is no tensile force sustainable in the bond. Once a bond fails, it is failed forever (there is no provision for "healing" of a failed bond); this makes the model history dependent. For purposes of illustration, consider the *prototype microelastic brittle* (PMB) material defined by

$$f(y(t),\boldsymbol{\xi}) = g(s(t,\boldsymbol{\xi}))\mu(t,\boldsymbol{\xi}), \tag{18}$$

where g is the linear scalar-valued function given by

$$g(s) = cs \quad \forall s, \tag{19}$$

where c is a constant and μ is a history-dependent scalar-valued function that takes on values of either 1 or 0

$$\mu(t,\boldsymbol{\xi}) = \begin{cases} 1 & \text{if } s(t',\boldsymbol{\xi}) < s_0 \quad \text{for all} \quad 0 \leqslant t' \leqslant t, \\ 0 & \text{otherwise.} \end{cases} \tag{20}$$

Here, s_0 is the critical stretch for bond failure, which for the moment will be assumed constant (Fig. 2). Note that although the PMB material is isotropic in its virgin state, breakage of bonds oriented in some particular direction will lead to anisotropy in subsequent response. One advantage of introducing failure at the bond level is that it leads to an unambiguous notion of local damage at a point, which is defined as

$$\varphi(\mathbf{x},t) = 1 - \frac{\int_{\mathcal{H}_\mathbf{x}} \mu(\mathbf{x},t,\boldsymbol{\xi})\,\mathrm{d}V_\xi}{\int_{\mathcal{H}_\mathbf{x}} \mathrm{d}V_\xi} \tag{21}$$

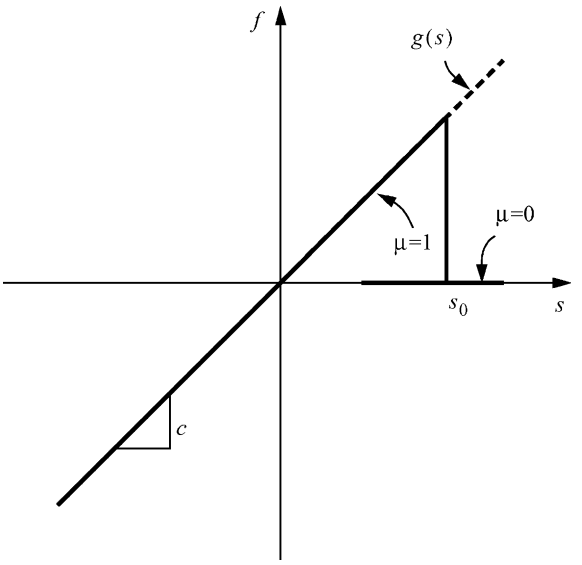

Fig. 2. Bond force as a function of bond stretch in the PMB material model.

in which $\mathbf{x}$ is now included as an argument of μ as a reminder that it is a function of position in the body. Note that $0 \leqslant \varphi \leqslant 1$, with 0 representing virgin material, and 1 representing complete disconnection of a point from all of the points with which it initially interacted.

Because broken bonds are unable to sustain tensile load, the onset of bond breakage at some point in a body leads to softening material response. This may cause an evolution of damage in which broken bonds coalesce into a surface that becomes a fracture, with extensive bond breakage across the surface. (The precise mathematical condition for material instability with regard to damage evolution is an open issue at this point. Such a criterion appears to be more complex in the present setting than loss of ellipticity in PDEs, especially because of the directional nature of damage due to bond failure introduced through $\mu(\mathbf{x}, t, \boldsymbol{\xi})$.)

Evidently there are only two parameters that characterize the PMB material, a "spring constant" c and the critical bond stretch s_0. The value of c corresponding to a given bulk modulus k is found as follows. Consider a large homogeneous body under isotropic extension, i.e., s is constant for all $\boldsymbol{\xi}$, and $\boldsymbol{\eta} = s\boldsymbol{\xi}$. Defining $\xi = |\boldsymbol{\xi}|$ and $\eta = |\boldsymbol{\eta}|$, we have $\eta = s\xi$. Using the definition of the micropotential (7), since $f = cs = c\eta/\xi$, it follows that $w = c\eta^2/2\xi = cs^2\xi/2$. Then, applying (8) leads to

$$W = \frac{1}{2}\int_{\mathscr{H}} w\,\mathrm{d}V_{\xi} = \frac{1}{2}\int_0^{\delta}\left(\frac{cs^2\xi}{2}\right)4\pi\xi^2\,\mathrm{d}\xi = \frac{\pi c s^2\delta^4}{4}. \tag{22}$$

This is required to equal the strain energy density in the classical theory of elasticity for the same material and the same deformation, $W = 9ks^2/2$. Combining this with (22) leads to the spring constant in the PMB material model [18]

$$c = \frac{18k}{\pi\delta^4}. \tag{23}$$

The critical stretch for bond failure, s_0, may also be related to a measurable quantity by considering a planar fracture surface in the interior of a large homogeneous body. To completely separate the two halves of the body across the fracture surface requires breaking all the bonds that initially connected points in the opposite halves. Let $w_0(\boldsymbol{\xi})$ denote the work required to break a single bond,

$$w_0(\boldsymbol{\xi}) = \int_0^{s_0} g(s)(\xi\,\mathrm{d}s), \quad \xi = |\,\boldsymbol{\xi}\,|, \tag{24}$$

where the relation $\mathrm{d}\eta = \xi\,\mathrm{d}s$ has been used. In the present case of the PMB material, (24) leads to $w_0(\boldsymbol{\xi}) = cs_0^2\xi/2$. The work G_0 required to break all the bonds per unit fracture area is then found from

$$G_0 = \int_0^{\delta}\int_0^{2\pi}\int_z^{\delta}\int_0^{\cos^{-1}z/\xi}(cs_0^2\xi/2)\xi^2\sin\phi\,\mathrm{d}\phi\,\mathrm{d}\xi\,\mathrm{d}\theta\,\mathrm{d}z. \tag{25}$$

(Refer to Fig. 3 for an explanation of this computation.) After evaluation of these integrals, the energy per unit fracture area for complete separation of the two halves of the body is found to be

$$G_0 = \frac{\pi c s_0^2\delta^5}{10}. \tag{26}$$

Since the energy release rate is a measurable quantity for brittle materials, (26) allows s_0 to be evaluated under the

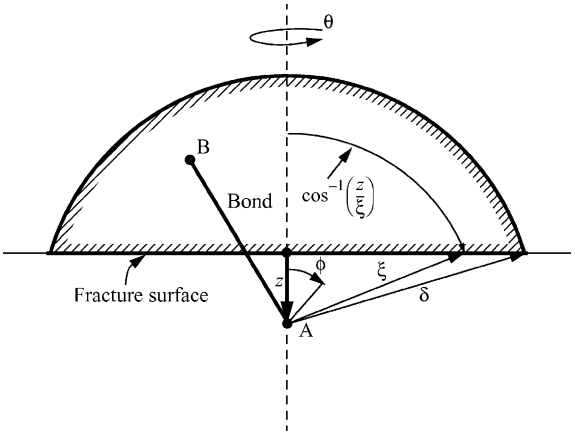

Fig. 3. Evaluation of fracture energy G_0. For each point A along the dashed line, $0 \leqslant z \leqslant \delta$, the work required to break the bonds connecting A to each point B in the spherical cap is summed by the integrals in Eq. (25) using a spherical coordinate system centered at A.

assumptions of complete separation of the fracture surfaces and of the absence of other dissipative mechanisms near the crack tip. Solving (26) for s_0 and using (23) leads to

$$s_0 = \sqrt{\frac{10G_0}{\pi c \delta^5}} = \sqrt{\frac{5G_0}{9k\delta}}. \tag{27}$$

This determines s_0 for the PMB material under the assumptions stated above.

For some real materials, it is an oversimplification to assume that the critical stretch for failure of a given bond is completely independent of conditions in all other bonds. For example, better agreement with experimental results on fracture in glass is obtained when the critical stretch s_0 in (20) is allowed to depend on $s_{\min}$, the current minimum stretch among all bonds connected to a given material point

$$s_0(t) = s_{00} - \alpha s_{\min}(t), \quad s_{\min}(t) = \min_{\xi}\left\{\frac{y(t) - |\,\xi\,|}{|\,\xi\,|}\right\}, \tag{28}$$

where s_{00} and α are constants, with α typically on the order of 1/4. Thus, compressive (negative) strains transverse to the direction of maximum stretch increase the critical stretch for bond failure. Other dependencies of s_0 could be introduced to model various effects that influence fracture behavior, such as environmental effects and manufacturing defects. Time-dependent behavior of s_0 can be introduced to model such effects as aging and fatigue.

Interfaces between materials are characterized through the properties of bonds that connect points in the different materials. The properties of these interface bonds can be chosen independently of the bonds within the individual materials. For example, a weak interface would be modeled by reducing s_0 for the bonds across the interface.

The model described above allows only one elastic constant, called c in the case of the PMB material, whereas linear elastic materials in the classical theory are characterized by two such constants. This difference occurs because an elastic solid that involves only two-particle interactions (a "Cauchy crystal") always has a Poisson ration of 1/4. A refinement of the peridynamic theory that allows dependence of strain energy density on local volume change in addition to two-particle interactions removes this restriction [8] but has not yet been implemented in the numerical method described in the remainder of this paper. Also under development are material models that incorporate permanent deformation at the bond level to model plastic response.

Another aspect of constitutive modeling in the peridynamic theory that has no analogue in the classical theory is the dependence of f on ξ. For the virgin PMB material, it was assumed for convenience that f depends only on s, which implies a particular dependence on ξ. However, many alternatives are possible, and it is shown in [8] that the nature of this dependence affects the dispersion relation of the material for linear waves. This can potentially be exploited in nanoscale modeling of materials.

4. Numerical method

The region is discretized into nodes, each with a known volume in the reference configuration. Taken together, the nodes form a grid. The method is meshfree in the sense that there are no elements or other geometrical connections between the nodes. For simplicity, the details of the method will be discussed below using the linearized version of the peridynamic theory applied to a homogeneous body. The discretized form of the equation of motion (1) replaces the integral by a finite sum:

$$\rho \ddot{\mathbf{u}}_i^n = \sum_p \mathbf{f}(\mathbf{u}_p^n - \mathbf{u}_i^n, \mathbf{x}_p - \mathbf{x}_i) V_p + \mathbf{b}_i^n, \tag{29}$$

where $\mathbf{f}$ is supplied by (11), n is the time step number, and subscripts denote the node number, so that

$$\mathbf{u}_i^n = \mathbf{u}(\mathbf{x}_i, t^n). \tag{30}$$

V_p is the volume of node p. To preserve the dimensions of quantities used in the threee-dimensional expression (1), it is helpful to assume that the one-dimensional problem refers to a bar of constant cross-sectional area A; thus $V_p = A\Delta x$, where Δx is the grid spacing, which is assumed to be constant. The sum in (29) is taken over all nodes p such that $|\mathbf{x}_p - \mathbf{x}_i| \leqslant \delta$.

The discretized form of the linearized peridynamic model is

$$\rho \ddot{\mathbf{u}}_i^n = \sum_p \mathbf{C}(\mathbf{x}_p - \mathbf{x}_i)(\mathbf{u}_p^n - \mathbf{u}_i^n) V_p + \mathbf{b}_i^n, \tag{31}$$

where $\mathbf{C}$ is defined in (15).

An explicit central difference formula is used for acceleration in either (29) or (31):

$$\ddot{\mathbf{u}}_i^n = \frac{\mathbf{u}_i^{n+1} - 2\mathbf{u}_i^n + \mathbf{u}_i^{n-1}}{\Delta t^2}, \tag{32}$$

where a constant time step size Δt is assumed.

Truncation error associated with the discretized model (31) can be analyzed in one dimension, assuming a homogeneous body:

$$\rho \ddot{u}_i^n = \sum_p C(x_p - x_i)(u_p^n - u_i^n) V_p + b_i^n, \tag{33}$$

where the micromodulus function is now a scalar-valued function C.

Under these assumptions, to derive the truncation error associated with (33), note that the equation of motion

$$\rho\ddot{u}(x_i) = \int_{-\delta}^{\delta} C(\xi)(u(x_i+\xi) - u(x_i))(A\,\mathrm{d}\xi) + b(x_i) \tag{34}$$

may be written without approximation in the form

$$\rho\ddot{u}(x_i) = A\sum_p \int_{-\Delta x/2}^{\Delta x/2} C(x_p - x_i + \xi)(u(x_p+\xi) - u(x_i))\,\mathrm{d}\xi + b(x_i). \tag{35}$$

(The argument t is dropped from u here to shorten the notation.) Under the assumption that the functions C and u are twice continuously differentiable, we can expand C near $x_p - x_i$ and u near x_p using the first few terms of a Taylor series:

$$C(x_p - x_i + \xi) = C(x_p - x_i) + C'(x_p - x_i)\xi + \mathrm{O}(\xi^2), \tag{36}$$

$$u(x_p + \xi) = u(x_p) + u'(x_p)\xi + \mathrm{O}(\xi^2). \tag{37}$$

Combining (35)–(37), and integrating leads to the conclusion

$$\rho\ddot{u}(x_i) = \sum_p C(x_p - x_i)(u(x_p) - u(x_i))V_p + b(x_i) + \mathrm{O}(\Delta x^2), \tag{38}$$

where use has been made of the fact that terms in the integrand that are linear in ξ integrate to 0. The error in the time difference formula (32) is well known to be $\mathrm{O}(\Delta t^2)$, so the conclusion is that the overall error in (33) is $\mathrm{O}(\Delta x^2) + \mathrm{O}(\Delta t^2)$.

However, when discontinuities in C or u are present, the assumption made prior to (36) that these functions are twice continuously differentiable no longer holds. In fact, the error changes under these conditions to $\mathrm{O}(\Delta x) + \mathrm{O}(\Delta t^2)$. The convergence study given in Section 5 illustrates the resulting linear rate of convergence in a crack growth problem, which necessarily contains discontinuities in $\mathbf{u}$.

A stability condition for the numerical scheme (33) will now be derived. Applying the standard assumption for a von Neumann stability analysis [19], let

$$u_i^n = \zeta^n \exp\left(\kappa \mathrm{i}\sqrt{-1}\right), \tag{39}$$

where κ is a positive real number and ζ is a complex number. The objective of the analysis is to determine a condition on Δt such that $|\zeta| \leqslant 1$ for all κ. This condition is necessary for waves not to grow unboundedly over time.

Using the notation $q = p - i$ and $C_q = C(x_p - x_i)$, the above assumptions when applied to (33) imply

$$\frac{\rho}{\Delta t^2}(\zeta - 2 + \zeta^{-1}) = \sum_{q=-\infty}^{\infty} AC_q\left(\exp\left(\kappa q\sqrt{-1}\right) - 1\right)\Delta x = \sum_{q=1}^{\infty} 2AC_q(\cos\kappa q - 1)\Delta x, \tag{40}$$

where the fact that C is an even function has been used in the last step. Now define

$$M_\kappa = \sum_{q=1}^{\infty} AC_q(1 - \cos\kappa q)\Delta x. \tag{41}$$

Then, using (40) and (41), and the quadratic formula to solve for ζ

$$\zeta = 1 - \frac{M_\kappa \Delta t^2}{\rho} \pm \sqrt{\left(1 - \frac{M_\kappa \Delta t^2}{\rho}\right)^2 - 1} \tag{42}$$

From this it is follows that the requirement $|\zeta| \leqslant 1$ implies:

$$\Delta t < \sqrt{2\rho/M_\kappa} \quad \forall\kappa. \tag{43}$$

To ensure that (43) holds for all wavenumbers κ, note that from (41)

$$M_\kappa \leqslant 2A\Delta x\sum_{q=1}^{\infty} C_q \tag{44}$$

hence the inequality (43) is satisfied whenever

$$\Delta t < \sqrt{\frac{\rho}{A\Delta x\sum_{q=1}^{\infty} C_q}}. \tag{45}$$

A more useful form of (45) is

$$\Delta t < \sqrt{\frac{2\rho}{\sum_p V_p C_{ip}}}, \tag{46}$$

where $C_{ip} = C(x_p - x_i)$. This form of the stability condition does not require the nodes to be numbered sequentially and is applicable to any number of dimensions by setting $C_{ip} = |\mathbf{C}(x_p - x_i)|$. Finally, for nonlinear material models, the appropriate form of the stability condition is (46) with $C_{ip} = |\partial\mathbf{f}/\partial\boldsymbol{\eta}|$. In this case it is important to apply a "safety factor" less than one to the stable time step to account for possible nonlinear material response that would make the estimated stable time step based on the linear analysis above too large.

A interesting feature of (46) is that for a given δ, the stable Δt is only weakly dependent on Δx. This is in contrast to the famous Courant–Friedrichs–Lewy condition that controls stability in conventional wavecodes, which requires that $\Delta t = \mathrm{O}(\Delta x)$ as $\Delta x \to 0$. However, it turns out that the dependence of C on δ implies that as δ is reduced, $\Delta t = \mathrm{O}(\delta)$. So, the maximum stable time step tends to be limited by the horizon rather than the grid spacing.

The value of δ may depend on the physical nature of the application being modeled. For example, at the nanoscale, δ would be determined by the distance over which physical interactions between atoms or molecules occur. However, in macroscale calculations, δ can be chosen according to convenience, since as shown previously, the parameters such as c that determine the bulk elastic properties of the material can be fitted to

experimental data for any value of δ. (See, for example, (23).) In practice for macroscale modeling, the value $\delta = 3\Delta x$ usually works well. Values much smaller than this typically result in undesirable grid effects (cracks grow along the rows or columns of the grid). Values much larger than this may result in excessive wave dispersion and require very large computer run times.

Boundary conditions are somewhat different in the peridynamic method than in the classical theory. As shown in [8], the variational formulation of the peridynamic equations does not lead to natural boundary conditions, which in the classical theory are traction boundary conditions. Instead, forces at the surface of a body must be applied as body forces **b** within some layer under the surface. In practice, this layer usually has thickness δ. Similarly, displacement boundary conditions must be prescribed within a layer of finite thickness under the surface.

Contact may be treated using short-range repulsive forces that prevent nodes from getting too close. These short-range forces are independent of the positions of the nodes in the reference configuration, so that contact is treated in a consistent way even under large deformation. This approach avoids the need for defining contact surfaces, as is required by many finite-element codes.

The discretized equation of motion (29) includes nonlinearity and damage at the bond level, since these are included in the constitutive model **f**. Recall that the history dependent variable μ in (20) is defined for each *bond* rather than merely for each *node*. Since the number of bonds is much larger than the number of nodes, computer memory requirements may be minimized by using a bit variable to store values of μ. Cracks initially present in a body are modeled by breaking each bond (the line segment connecting a pair of nodes) that intersects the surface of the crack. Here, "breaking a bond" means setting the corresponding bit variable μ to 0 rather than 1 initially.

Although the above analysis assumes a regular lattice of nodes, the method is not restricted to such structured grids. Irregular grids may be used, the only complication being the need to define a volume associated with each node. This may be accomplished using computational geometry techniques such as Delaunay triangulation or Voronoi diagrams [20]. A less accurate but much simpler approach is to set the nodal volume based on the distances of a given node to some small set of its nearest neighbors. Using irregular grids, complex geometries may be modeled, and the full advantages of a meshfree method are realized.

5. Example problem: Convergence in a fracture calculation

In this section, the convergence of the method as grid spacing is reduced is demonstrated for a nonlinear problem that includes damage and fracture. Crack initiation, growth, and arrest are all involved in this problem, providing insight into convergence of the numerical method for practical applications involving dynamic fracture.

Consider a thick square plate (Fig. 4) of side length 50 mm, containing a center crack of initial length $2a_0 = 10$ mm. The material density is 8000 kg/m^3, and Young's modulus is 192 GPa. A constant horizon $\delta = 1.6$ mm is assumed, which is slightly greater than $3\Delta x$ for the case of the coarsest grid studied. The PMB material model is used with a constant value of the critical stretch for bond failure, $s_0 = 0.02$. Velocity boundary conditions are applied as shown in Fig. 5 consisting of a tensile square pulse followed by a compressive square pulse. The velocities are applied symmetrically on the horizontal edges of the plate within strips of width δ. The first pulse creates tensile stress waves that move toward the crack, creating mode-I loading at the crack tips. The duration of the tensile pulse is 5.0 μs, during which interval the crack grows. The growth is straight because of the symmetry of the problem. The tensile pulse is followed by a compressive pulse that stops the crack growth. Fig. 6 shows contours of elastic energy density at time 6.7 μs, as the crack is growing. As would be expected, the highest elastic energy density is found ahead of the crack tips.

The calculation was carried out with all parameters held constant, but four different values of grid spacing, $\Delta x = 0.10$ mm, 0.25 mm, 0.35 mm, and 0.50 mm. The grid in all cases was a square lattice with uniform spac-

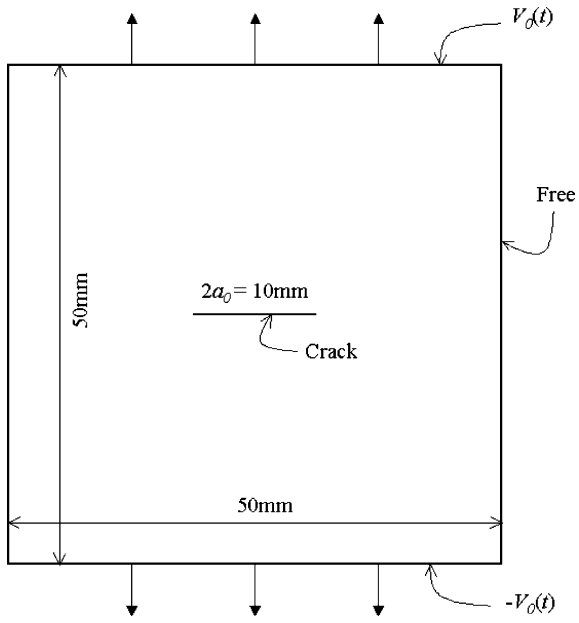

Fig. 4. Square plate containing an initial center crack.

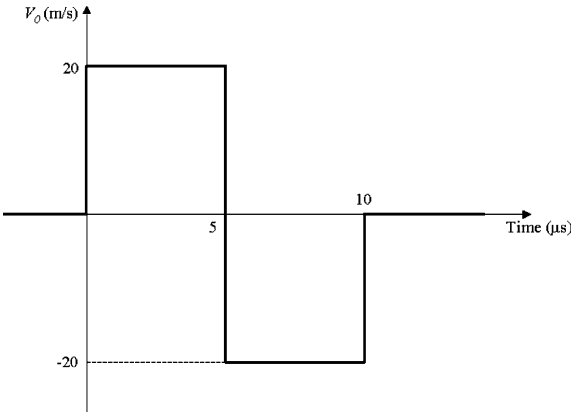

Fig. 5. Velocity applied to plate horizontal edges.

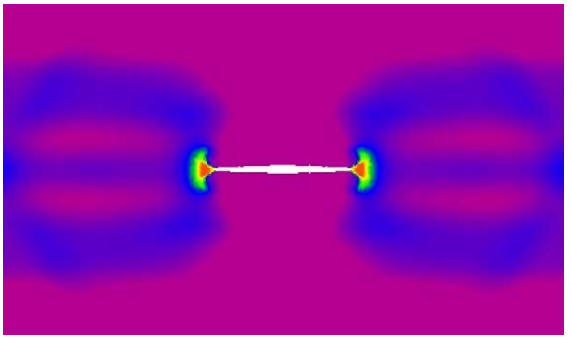

Fig. 6. Contours of elastic energy density as the crack grows.

ing throughout. The resulting predictions for crack growth distance Δa as a function of time are shown in Fig. 7. The crack tip position at any time is defined to be the maximum value of x_1 among all nodes i such that $\varphi_i > \varphi_0$, where φ_i is the nodal value of damage defined in (21), and $\varphi_0 = 0.3$. (This value of φ_0, although slightly arbitrary, was chosen because φ usually reaches a maximum of about 0.4 along the crack faces.) The stairstep appearance of the curves for the coarser grids occurs because, using this definition, the crack tip position jumps discontinuously by Δx as the crack grows over time.

The maximum predicted crack growth speed (obtained from the slope of the curves in Fig. 7) is about 1300 m/s, which is less than the Rayleigh wave speed (2800 m/s). The predicted crack growth speed is therefore well within the theoretical limit for steady mode-I fracture [21].

Fig. 7 shows that variations in the predicted crack initiation time, arrest time, total growth distance, and velocity, are on the order of the variations in grid spacing. This demonstrates in a practical sense the linear convergence of the predicted dynamic fracture behavior as Δx is reduced.

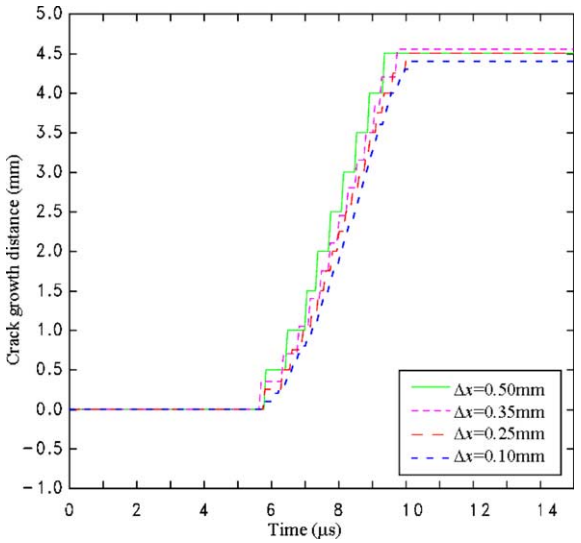

Fig. 7. Crack tip growth distance $\Delta a(t)$ predicted with four different grid spacings.

6. Example problem: impact of a sphere on a brittle target

Consider the impact of a rigid sphere against a homogeneous block of brittle material. The sphere has mass 4.16 gm, diameter 10 mm, and impact velocity 35 m/s directed normal to the target surface. The target material has density $\rho = 2200$ kg/m^3. The PMB material model is used for the target with bulk modulus $k = 14.9$ GPa and a critical bond stretch for failure given by (28) with $s_{00} = 0.0005$ and $\alpha = 0.25$. A three-dimensional cubic grid with spacing $\Delta x = 0.5$ mm and horizon $\delta = 1.50$ mm is used. The target is a cylinder with diameter 34 mm and height 25 mm. The target grid contains approximately 185,000 nodes and has free surfaces at the boundaries.

Fig. 8 shows two views of the predicted crack. The plot on the left shows a cross-section of the target after the projectile has rebounded, showing damage contours in the target material, where damage is the quantity φ defined in (21). The damage is localized in a cone-shaped surface which is known as a Hertzian crack. A three-dimensional view of this crack is shown on the right. The curvature near the circular crack tip is presumably due to interaction with the free cylindrical surface. The formation of conical Hertzian cracks in glass under impact by spheres is observed experimentally, for example by Ball [22].

Predictions for a similar problem, but with impact velocity 100 m/s and a target with diameter 74 mm and thickness 2.5 mm, are shown in Fig. 9. The upper plot shows the classic debris cloud of high-velocity impact on a thin target. The lower plot omits the small debris and shows the predicted fragmentation of the entire target (displacements are exaggerated by a factor of 5). This illustrates the ability of the method to model complex patterns of crack growth and mutual interaction.

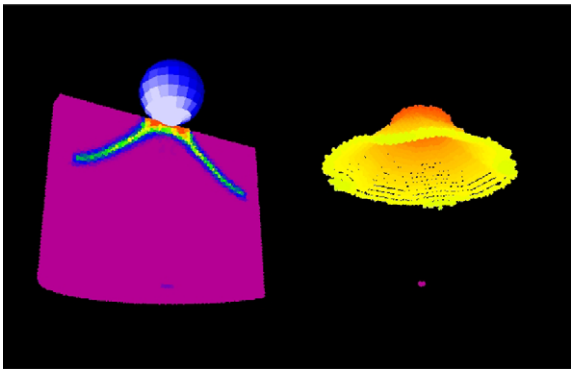

Fig. 8. Hertzian cracks due to impact on a brittle solid: (left) Cross-section showing damage contours and (right) conical crack.

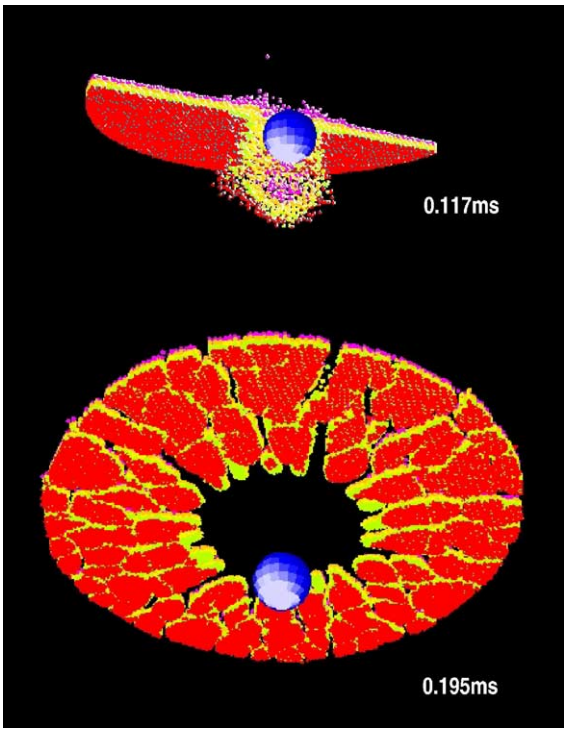

Fig. 9. Debris cloud and fragmentation due to impact on a thin brittle target.

An additional example concerned with dynamic fracture in a high-strength steel plate may be found in [10]. Other examples may be found in [11,12].

7. Discussion

The primary advantage of the peridynamic approach to fracture modeling is that it does not require any supplemental relation that dictates when a crack should grow, its velocity, direction, branching and instability, and arrest. All of these phenomena emerge as consequences of the equation of motion and the constitutive model, which incorporates damage at the bond level. In particular, it is not necessary to evaluate a stress intensity factor at a crack tip for use in such a supplemental relation, or even to keep track of the crack tip's position. Because the same underlying equations apply either on or off of a crack surface, it is unnecessary to treat opposite sides of a crack separately. For these reasons, any number of cracks can be treated, including all their mutual interactions.

The question of the validity of the underlying integral equations with respect to experimental data is beyond the scope of this paper. However, it is worth noting that these equations have been shown [9] to converge to the classical PDEs, at least in the limited case of a one-dimensional linear elastic bar, as the horizon shrinks, $\delta \to 0$. Also, any microelastic peridynamic constitutive model has an equivalent in the classical theory, in the sense of having identical response under homogeneous deformation [8]. The ability to prescribe, at least approximately, an energy release rate (27) makes a connection between the present theory and established principles of fracture mechanics.

As noted in the Introduction, several meshfree methods such as SPH have been proposed as a means to model fracture. There are fundamental distinctions in both theory and practice between these methods and the one proposed here. The main theoretical difference is that the peridynamic approach solves a different set of continuum equations. The integral equations of the peridynamic model remain directly applicable when a discontinuity appears, while the PDEs of the classical theory do not. The practical difference is that cracks emerge spontaneously in a peridynamic model as a natural consequence of the equation of motion and constitutive models. Another practical difference is that the peridynamic model is based on interactions between pairs of nodes, and therefore does not require a statistically large population of neighboring nodes to determine spatial derivatives. One consequence of this pairwise approach is that the peridynamic method does not suffer from the well-known "tensile instability" in SPH.

A promising alternative numerical model based on the peridynamic theory, with particular application to fracture and failure of reinforced concrete, is under development by Gerstle [23]. Another numerical approach, which may result in improved accuracy, is being investigated by Emmrich and Weckner [24].

Acknowledgement

Sandia is a multiprogram laboratory operated by Sandia Corporation for the United States Department

of Energy under Contract DE-AC04-94AL85000. This work was supported by the Joint DOE/DOD Munitions Technology Program, by the U.S. Nuclear Regulatory Commission, by the US Department of Energy, and by The Boeing Company. Discussions with John Chumley of Techneglas, Inc. regarding Hertzian cracking are gratefully acknowledged. The authors thank Professor Walter Gerstle for helpful discussions and for providing a correction to Eq. (23).

References

[1] Randles PW, Libersky LD. Smoothed particle hydrodynamics: some recent improvements and applications. Comput Methods Appl Mech Eng 1996;139:375–408.
[2] Krysl P, Belytschko T. The element free Galerkin method for dynamic propagation of arbitrary 3-D cracks. Int J Numer Methods Eng 1999;44:767–800.
[3] Carpinteri A, Ferro G, Ventura G. An augmented Lagrangian element-free (ALEF) approach for crack discontinuities. Comput Methods Appl Mech Eng 2001;191:941–57.
[4] Li S, Liu W-K, Qian D, Guduru PR, Rosakis AJ. Dynamic shear band propagation and micro-structure of adiabatic shear band. Comput Methods Appl Mech Eng 2001;191:73–92.
[5] Chen YP, Lee JD, Eskandarian A. Dynamic meshless method applied to nonlocal crack problems. Theoret Appl Fract Mech 2002;38:293–300.
[6] Rao BN, Rahman S. Mesh-free analysis of cracks in isotropic functionally graded materials. Eng Fract Mech 2003;70:1–27.
[7] Oliver J, Huespe AE. Continuum approach to material failure in strong discontinuity settings. Comput Methods Appl Mech Eng 2004;193:3195–220.
[8] Silling SA. Reformulation of elasticity theory for discontinuities and long-range forces. J Mech Phys Solids 2000;48:175–209.
[9] Silling SA, Zimmermann M, Abeyaratne R. Deformation of a peridynamic bar. J Elast 2003;73:173–90.
[10] Silling SA. Dynamic fracture modeling with a meshfree peridynamic code. In: Bathe KJ, editor. Computat Fluid Solid Mech. Amsterdam: Elsevier; 2003. p. 641–4.
[11] Silling SA, Askari E. Peridynamic modeling of impact damage. In: Moody FJ, editor. PVP-Vol 489. New York: American Society of Mechanical Engineers; 2004. p. 197–205.
[12] Silling SA, Bobaru F. Peridynamic modeling of membranes and fibers. Int J Non-Linear Mech 2005;40:395–409.
[13] Weckner O, Abeyaratne R. The effect of long-range forces on the dynamics of a bar. J Mech Phys Solids 2005;53:705–28.
[14] Kunin IA. Elastic media with microstructure I: one-dimensional models. Berlin: Springer-Verlag; 1982. p. 27.
[15] Rogula D. Nonlocal Theory of Material Media. Berlin: Springer-Verlag; 1982. p. 137–49, 243–78.
[16] Eringen AC, Speziale CG, Kim BS. Crack-tip problem in non-local elasticity. J Mech Phys Solids 1977;25:339–355.
[17] Ozbolt J, Bazant ZP. Numerical smeared fracture analysis: nonlocal microcrack interaction approach. Int J Numer Methods Eng 1996;39:635–61.
[18] The version of this equation that appears in [11] contains an error.
[19] Lapidus L, Pinder GF. Numerical solution of partial differential equations in science and engineering. New York: Wiley; 2003. p. 171.
[20] Okabe A, Boots B, Sugihara K, Chiu SN. Spatial tesselations: concepts and applications of Voronoi diagrams. New York: Wiley; 2000.
[21] Yoffe EH. The moving Griffith crack. Philos Mag 1951;42:739–50.
[22] Ball A. On the bifurcation of cone cracks in glass plates. Philos Mag A 1996;73:1093–103.
[23] Gerstle W, Sau N, Peridynamic modeling of concrete structures. In: Li L, editor. Proceedings of the Fifth International Conference on Fracture Mechanics of Concrete Structures, Ia-FRAMCOS, vol. 2; 2004. p. 949–56.
[24] Emmrich E, Weckner O, Analysis and numerical approximation of an integro-differential equation modelling nonlocal effects in linear elasticity [to appear].